Interparticle Forces of a Native and Encapsulated Metal-Organic Framework and Their Effects on Colloidal Dispersion

E. L. Butler,[†] B. Reid,[‡] P. F. Luckham,[¶] S. Guldin,[*,‡] A.G. Livingston,[§] and C. Petit[*,§]

[†]*Barrer Centre, Department of Chemical Engineering, Imperial College London, London, SW7 2AZ, UK*

[‡]*Department of Chemical Engineering, University College London, Torrington Place, London, WC1E 7JE, UK*

[¶]*Department of Chemical Engineering, Imperial College London, London, SW7 2AZ, UK*

[§]*Barrer Centre, Imperial College London, London, SW7 2AZ, UK*

E-mail: s.guldin@ucl.ac.uk; camille.petit@imperial.ac.uk

Abstract

The colloidal properties suspended of metal-organic frameworks (MOFs) are critical for device fabrication and application. Herein, van der Waals attractive, electric double layer repulsive and steric repulsive forces of a native and encapsulated MOF are quantified for the first time. The van der Waals attractive forces were investigated by conducting environmental ellipsometric porosimetry (EEP) and spectroscopic ellipsometry (SE) on sub-micron, optical-quality nanoparticle films. The repulsive forces were determined from colloid and material characterization measurements. These data were used to predict suspension properties via extended Derjaguin, Landau, Verwey

and Overbeek theory. The state of dispersion was quantified for comparison with theoretical predictions for nine solvents. The MOF encapsulated with a surface-selective modification showed superior suspension in hydrophobic solvents. These findings should expedite the formulation of MOF colloidal suspensions for future works.

Keywords

Metal Organic Frameworks (MOFs); Colloids; Thin Films; Surface Functionalization; Environmental Ellipsometric Porosimetry (EEP)

1 Introduction

Through mastering the assembly of metal clusters and organic ligands, scientists have developed a class of molecularly defined materials with record-breaking material properties: metal-organic frameworks (MOFs).[1–6] For widespread implementation of MOFs in a variety of applications, it is imperative to understand their colloidal behavior and surface properties. For drug delivery, surface properties and dispersion play a critical role in affecting where particles travel to in the body.[7] The efficacy of catalysis and adsorption also depends on interfacial phenomenon of MOF particles.[8,9] Moreover, MOF colloidal properties during device fabrication affect the device's ultimate performance. During mixed matrix membrane fabrication, MOF aggregates and poor MOF-polymer contact lead to non-selective defects and embrittlement.[10] Similar issues arise in composite MOF materials used for catalysis, gas storage and separation. The performance of MOF devices made by depositing colloidal MOFs can suffer from poor colloidal control. These include optical, electronic and chemical sensing devices.[11,12] While there are many articles exploring applications of colloidal MOFs, there are few articles dedicated to the colloidal properties of MOFs. The majority of these focus on modifying the surfaces of MOF particles with phosphates,[13] polymers,[7,14] which are attached either covalently to coordinatively unsaturated sites or through van der Waals

forces. Some of these studies demonstrated control of MOF colloidal particles, while others did likewise without modification.[15–17]

These findings are of significant interest; however, the authors are unaware of any work to date which explores and quantifies the fundamental surface property parameters of MOF particles. Instead, many studies rely on a trial and error approach to formulate colloidal suspensions for the aforementioned applications. While many positive results have been achieved, a faster, more effective approach based on the fundamentals of colloid and interface science would be of great utility to this now large body of research. We address this knowledge gap by applying principles of colloid science to MOF particles and asking: what interparticle forces are important for colloidal MOFs? We captured the motivation of this study is Scheme 1. To explore this question, three interparticle forces were investigated: van der Waals attractive forces, electric double layer repulsive forces and steric repulsive forces, as defined by an extended Derjaguin, Landau, Verwey and Overbeek (DLVO) equation (Section S1.1, Supporting Information). We note that the 'steric' term, although used here, is rather quantitative, since today no satisfactory analytical expression exists. MIL-101 was chosen for initial study as an analogue for carboxylate MOFs, because similar MOFs demonstrate high porosity and hydrolytic stability.[18] According to DLVO theory, MIL-101 should suspend well in high dielectric constant solvents and poorly in low dielectric constant solvents. Moreover, by leveraging the unique chemistry of MIL-101, it may be possible to enhance its suspension in low dielectric constant solvents with a post-synthetic modification that adds an additional steric repulsive force.

2 Experimental

2.1 Metal-Organic Framework Synthesis

MIL-101 was synthesized similarly to previous studies.[19,20] 1.35 g of chromium(III) chloride hexahydrate ($CrCl_3 \bullet H_2O$), purum p.a., >98%, Aldrich Chemistry) was weighed (Adventurer

Pro Model: AV114CM, Ohaus) and placed in a vessel (XP 1500 Plus, CEM Corporation) with 50 mL of DI (deionized) water (Centra R200, Elga). 0.865 g of terepthalic acid (TPA, 98%, Sigma-Aldrich) was then added and the solution was stirred. This was repeated for twelve vessels, which were loaded into the microwave (MARS 5 Microwave Digestion Oven, CEM Corporation) and heated to 180 °C within 10 minutes and held at that temperature for an additional 30 minutes. The vessels were cooled to room temperature inside the microwave. The contents of each vessel were centrifuged at 15,000 rcf for 30 minutes (Centrifuge 5810R, Eppendorf). The supernatant was then decanted. The product was re-suspended in water and re-centrifuged three times. The same process was used for dimethylformamide (DMF). The washed contents of each centrifuge tube were combined in a flask, submerged in 300 mL of DMF (AnalaR Normapur, VWR) and stirred overnight at 120 °C. In the morning, the product was centrifuged as before and washed three times with MeOH (AnalaR Normapur, VWR). The product was then refluxed in 300 mL of MeOH overnight. Finally, it was centrifuged, air dried at 60 °C for several hours, and dried in a vacuum oven (Vacutherm vacuum oven, ThermoFisher Scientific) at 120 °C overnight. The dry powder was stored in a desiccator.

2.2 Suspension Preparation

MIL-101 was dried overnight in a vacuum oven at 120 °C and then cooled under flowing dry nitrogen (Research Grade, BOC). Then, the MIL-101 was weighed and an appropriate amount of solvent was added. To achieve suspension, the solutions were sonicated in pulse mode for 60 minutes at 37 kHz, 100% power, and ambient temperature before being left to stir overnight. In the morning, the samples were freshly sonicated under the same conditions and left to stir for one hour before any analysis. The solvents used for suspension included: DI water, MeOH, DMF, BuOH (AnalaR Normapur, VWR), n-decanol (DeOH, 99%, Aldrich Chemicals), Hex (AnalaR Normapur, VWR), DCM (GPR Rectapur, VWR), EA (GPR Rectapur, VWR), Act (GPR Rectapur, VWR) and IsoPar G (Brenntag).

2.3 Post-Synthetic Modification of Metal-Organic Framework

1 g of MIL-101 was dried in a vacuum oven at 120 °C overnight and cooled under dry nitrogen. The cooled MIL-101 was added to a dry flask and three vacuum-argon (Research Grade, BOC) flushes were conducted. 100 mL of toluene (Tol, AnalaR Normapur, VWR) dried with molecular sieves (4Å, VWR) was added to suspend the MIL-101 and finally 1.7 mL of 1-octylamine (OA, 99%, Aldrich Chemicals) or 1 g of amine terminated polystyrene (ATPS, Mn = 10,000, Sigma-Aldrich) was added to the suspension. This suspension was sonicated at 80 °C for 2 hours at 100% power and 37 hz in pulse mode (Elmasonic P, Elma). Then it was allowed to stir at reflux for 5 hours. Finally, the product was centrifuged and washed three times with toluene, similar to the washing procedure conducted after the synthesis. Finally, the product was dried in a vacuum oven at 120 °C overnight.

2.4 Optical-Quality Metal-Organic Framework Film Fabrication

Prior to dip coating, the silicon substrate was cleaned with 1 M aqueous sodium hydroxide (NaOH, >98% pellets (anhydrous), Sigma-Aldrich) and EtOH (absolute, GPR Rectapur, VWR) by sonicating the substrates in each using pulse mode for 30 minutes at 37 hz and 100% power. The substrate was dried in an oven (Heratherm Oven, Fisher Scientific) in a glass petri dish at 120 °C. The substrate was then dip coated at room temperature at withdrawal speeds of 0.5 to 50 $mm.m^{-1}$ (RDC15 Dip Coater, Bungard) into MIL-101 suspensions between 500 ppmv and 10.5% ($v.v^{-1}$) in MeOH and DMF.

2.5 Metal-Organic Framework Powder Characterization

Prior to all characterization, the samples were degassed overnight at 120 °C in a vacuum oven and cooled under dry nitrogen. The samples were then promptly weighed and subjected to characterization. For nitrogen sorption measurements, the samples were further degassed (VacPrep 061 Sample Degas System, Micromeretics) overnight at 120 °C and 0.2 mbar and

then degassed in situ for 4 hours at 120 °C and 0.003 mbar. Nitrogen gas adsorption was performed (Flex Surface Characterization System, Micromeritics) at 77.4 K and the BET method was used for analysis.[21] XRD was performed using a Ni filter and Cu-α radiation at 40 kV and 40 mA (X'Pert Pro XRD, PANanalytical). FTIR was performed at a 2 cm^{-1} resolution and 1 cm^{-1} sampling interval for 16 trials per sample (Spectrum 100, PerkinElmer). MOF data are presented in the main paper. SEM images were processed for particle size distribution and surface coverage (ImageJ, NIH). The final data, presented in Figure 1B, was determined from 40 data points from images similar to Figure S2. Note that doublets were excluded from the calculation. These images were created by dip coating silicon wafers in 100 ppmv MeOH at 5 $mm.m^{-1}$. For TGA, samples were heated from 25 to 900 °C at 10 $°C.m^{-1}$ under air and nitrogen flow rates of 96 and 33 cm^3 $(STP).m^{-1}$, respectively (TG209F1 Libra, Netzsch). XPS was conducted (K-Alpha+TM, Thermo ScientificTM) using a Kα monochromated X-ray source (MXR3 Al, $h\nu$ = 1486.6 eV). The power was set to 72 W using a 20 eV pass energy and 0.1 eV step size. Samples were mounted on carbon tape. Data was analyzed (Thermo Advantage, Thermo Scientific) after normalizing the binding energies to the adventitious carbon peak (284.8 eV). Sample counts were normalized to the peak maximum of chromium when compared.

2.6 Metal-Organic Framework Colloidal Characterization

Zeta potential measurements were carried out on 300 ppmv suspensions of MIL-101 in select solvents at 25 °C using the solvent parameters listed in Table S1 and the Smoluchowski model[22] for analysis (PALS Zeta Potential Analyser, BI-SERL Electrode Assembly, BI-SCGO Glass Cuvettes, Brookhaven Instruments Corporation). The critical point of aggregation was assessed using UV-visible spectrophotometry (UV-1800 UV Spectrophotometer, Shimadzu). Suspensions between 10 and 3000 ppmv of MIL-101 were prepared and the absorbance was measured as a function of wavelength (375 – 525 nm) in quartz cuvettes (Quartz SUPRASIL® High Precision Cell, 10 mm light path, Hellma Analytics). Note that this is a

non-absorbing region for MIL-101 and the solvents chosen. The method of analysis is based on that developed by Heller et al. and demonstrated by other authors.[23–26] They state that specific absorbances (A/C) of dilute colloidal suspensions are a function of wavelength (λ):

$$\frac{A}{C} = m\lambda^{-z} \tag{1}$$

where m is a constant that is a function of particle size and relative refractive index and z is the wavelength exponent. The wavelength exponent of a suspension can be estimated as the slope of a log-log plot of specific absorbance versus wavelength, since the above equation can be manipulated to show:

$$z = -\left(\frac{d\log(A/C)}{d\log(\lambda)}\right) + \left(\frac{d\log(m)}{d\log(\lambda)}\right) \tag{2}$$

Note that m is constant over small wavelength ranges, like those used in this work, so the second term is effectively equivalent to zero. While this technique has become less common, it is still a sensitive technique for assessing particle aggregation. The wavelength exponent should remain constant for well-dispersed particles and decrease with increasing aggregate size. The point of interception between the constant wavelength exponent region and decreasing wavelength exponent region is considered the critical point of aggregation.

2.7 Metal-Organic Framework Film Characterization

First, the MIL-101 nanoparticle films were qualitatively analysed with scanning electron microscopy (SEM) imaging. Experiments were performed at 5 kV (LEO 1525, Karl Zeiss) and samples were mounted with carbon tape and coated with 15 nm of chromium at 120 mA (Q150T S Plus, Quorom Technologies). Atomic force microscopy (AFM) was conducted (Dimension Icon, Bruker) using a silicon probe with a <12 nm tip radius, 70 kHz response frequency and 0.4 N.m^{-1} spring constant (ScanAsyst, Bruker). A resolution of 256 point per line on less than 3 x 3 μm areas were used with a 0.4 Hz scan rate. The images were

flattened and cleaned with data visualization software and root-mean-square roughness (R_q) was calculated (Gwyddion 2.44 SPM). Spectroscopic ellipsometry (SE) and environmental ellipsometry porosimetry (EEP) measurements were performed using a spectroscopic ellipsometer (SE2000 Modular Optical Platform, Semilab) and analysed with the software of the manufacturer (SEA).[27] All measurements were carried out at an incident angle of 73 ° on a silicon substrate corresponding to the approximate Brewster angle of the substrate. Measurements were conducted at ambient temperatures after drying the samples on a hot plate for 5 minutes at 120 °C. SE measurements were taken prior to EEP measurements. Data fitting was performed using a standard Cauchy dispersion law in the non-absorbing regions of the spectra. During EEP measurements, the refractive index was obtained at each humidity point to generate an adsorption-desorption isotherm. The adsorption-desorption isotherm enabled the derivations of the relative adsorbed solvent volume and corresponding absolute porosity. From the isotherms, we also derived pore radius distribution via a Lorentz-Lorentz effective medium approximation and a modified Kelvin formula, respectively.[28,29] These data are presented in Figure 2.

3 Results and Discussion

The van der Waals attractive forces are directly proportional to the Hamaker constant (Section S1.2, Supporting Information). One must calculate the latter to apply DLVO theory. This calculation requires the experimental determination of spectral parameters. While these parameters are readily available in the literature for solvents used in this study, none have been measured for MOFs. Herein, we combine SE with EEP to assess the optical properties and porosity of a MIL-101 film. Combining these techniques, it is possible to approximate the Hamaker constant and hence the van der Waals attractive forces of MIL-101 in any fluid environment (Sections S1.2 and S5.4, Supporting Information). To pursue this approach, optical-quality, nanoparticle films of MIL-101 were synthesized (Section S2.4, Supporting

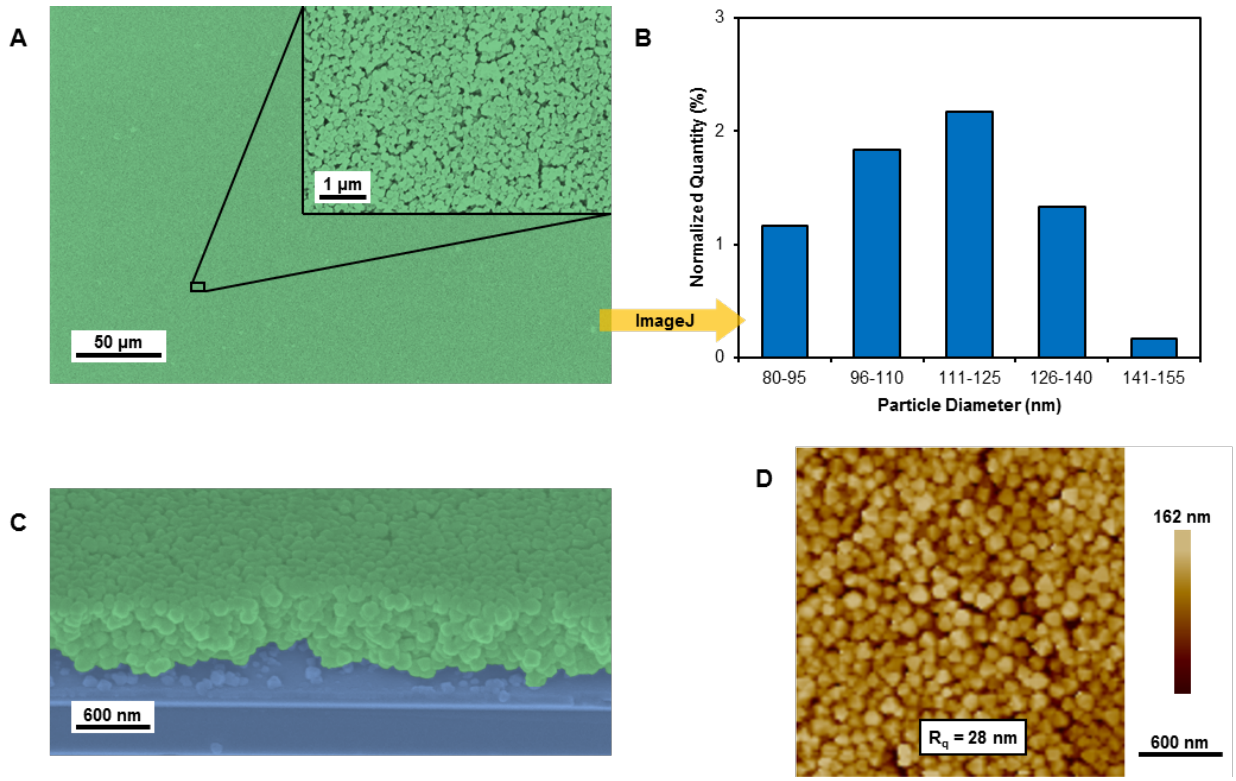

Figure 1: Morphological characterization of MIL-101 thin particle films used to determine the spectral parameters of MIL-101 in the UV-Vis range. (A) Surface SEM images with colored silicon (blue) and MIL-101 (green). (B) Particle size distribution from ImageJ analysis. (C) 45 ° angled SEM cross-section image. (D) AFM image.

Information) and characterized (Section S5, Supporting Information) for uniformity and surface roughness, as these are critical parameters in achieving good ellipsometric measurements. After an initial study (Section S5.2, Supporting Information), films were successfully synthesized by dip coating silicon wafers in 7.9% v/v MIL-101 in N,N-dimethylformamide (DMF) suspensions at a withdrawal speed of 1.0 mm.min^{-1}. As shown in Figures 1A and 1D, complete surface coverage was achieved over a large area with a reasonably low root mean square surface roughness (R_q) of 28 nm. This low surface roughness should not significantly interfere with the ESE measurements as it is more than an order of magnitude smaller than the wavelength of light used for analysis.

After confirming nanoparticle film quality, SE measurements were conducted and a Cauchy dispersion model was applied to the data to obtain film thickness and refractive

index values. For cross-validation, the film's modelled thickness of ≈1 μm was verified by taking a 45 ° cross-sectional SEM image (Figure 1C). As presented in Figure 1B, the mean particle diameter was 113 nm with a standard deviation of 17 nm (Figure 1B), implying a film thickness equivalent to ≈9 particle diameters. To determine the interparticle voidage, the water vapor isotherm measured via EEP was interrogated. Figure 2A shows that the film follows a type V isotherm at partial pressures below 0.95 with an H1 type of hysteresis, which is typical of capillary condensation inside pores.[30] Moreover, it remains relatively flat between partial pressures of ≈0.5 until ≈0.8, after which it increases. This latter region can be attributed to the mesoporous region of this film created by dense particle packing, while the two-heeled vapor sorption between ≈0.3 and ≈0.5 can be attributed to microporosity of the particles. As shown in Figure 2B, pore size distributions from the ≈0.3 to ≈0.5 region can be calculated using the Kelvin model for water sorption into pores (See Section S5.4, Supporting Information). The porosimetry data demonstrate two median radii of ≈1.50 and ≈1.75 nm, within 7% error of the theoretical pore radii.[18] These results are particularly encouraging as to-date little data exists on the validity of environmental ellipsometric porosimetry for MOF films.[31,32] By comparing the relative water uptake of this film and bulk measurements of MIL-101 at a partial pressure of 0.59, one can calculate an interparticle void volume fraction of 0.43 (Section S5.4, Supporting Information). A total void fraction in the MIL-101 film of ≈0.90 can be calculated by adding the interparticle void volume fraction to MIL-101's porosity. This value was used in the final model to determine the refractive index of MIL-101's skeletal framework as a function of wavelength.

The optical data were transformed into a Cauchy plot, Figure 2C, and a linear regression was performed to determine the spectral parameters: C_{UV} = 5.36 and ω_{UV} = 7.14 x 1015 rad.s^{-1}, comparable to similar inorganic materials.[33] These values define the skeletal structure of MIL-101 and are not indicative of bulk properties. The spectral parameters can be used to calculate the Hamaker constant of MIL-101 in different environments. A Hamaker constant of 3.31 x 10^{-21} J was found for MIL-101 in vacuum and MIL-101's Hamaker con-

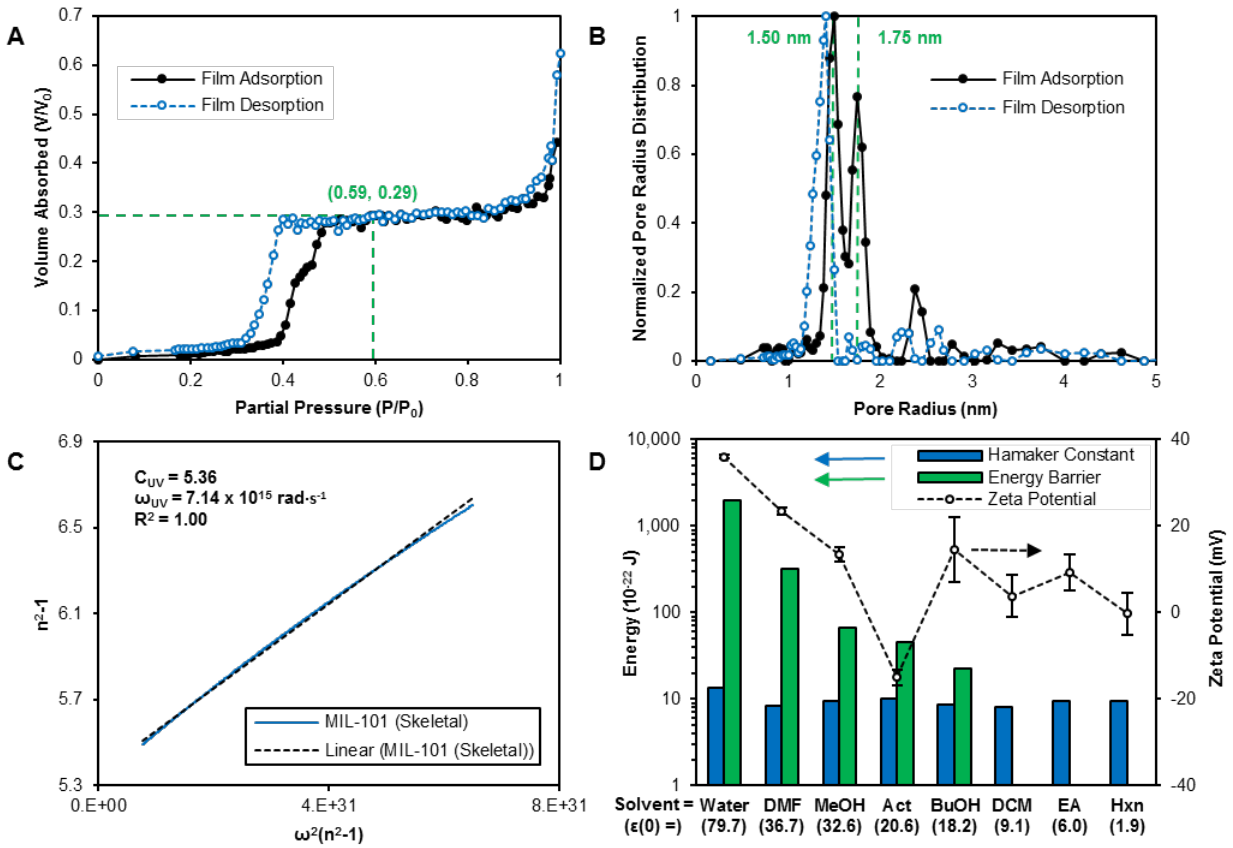

Figure 2: The determination of van der Waals attractive and electric repulsive forces and the resulting predictions. (A) EEP water sorption measurements, (B) the resulting pore size distribution and (C) Cauchy plot of the skeletal MIL-101 spectral data. (D) Dielectric constants [$\epsilon(0)$], zeta potentials, Hamaker constants and DLVO energy barrier maxima. Green, dashed lines mark the point at which water sorption is complete in MIL-101's pores and the median pore sizes of MIL-101 in (A) and (B), respectively. All measurements were taken at room temperature unless otherwise stated in the Supporting Information.

stant in selected solvents are shown in Figure 2D. Dielectric constant, zeta potential and energy barrier data are also included in the same figure. The Hamaker constants have a narrow range between 0.80 and 1.33 • 10^{-21} J, with dichloromethane (DCM) being the lowest and water being the highest. These values are relatively low,[33] which can be attributed MIL-101's large voidage (Section S1.2, Supporting Information). The absolute value of the zeta potential decreases with decreasing solvent dielectric constant. Energy barriers can be calculated using the values in Figure 2D using the classic DLVO equation (Section S1.1, Supporting Information). If the electric double layer repulsive forces are strong enough, an

energy barrier maintains a reasonable colloidal dispersion, as highlighted by the green dashed line in Figure 3. However, if the electric double layer repulsive forces are sufficiently low, the van der Waals attractive forces will dominate. This leads to unstable colloidal suspensions, highlighted by the black solid line. Since the electric double layer repulsive forces are proportional to the dielectric constant and the square of zeta potential, the calculated energy barrier decreases rapidly as these quantities decrease.

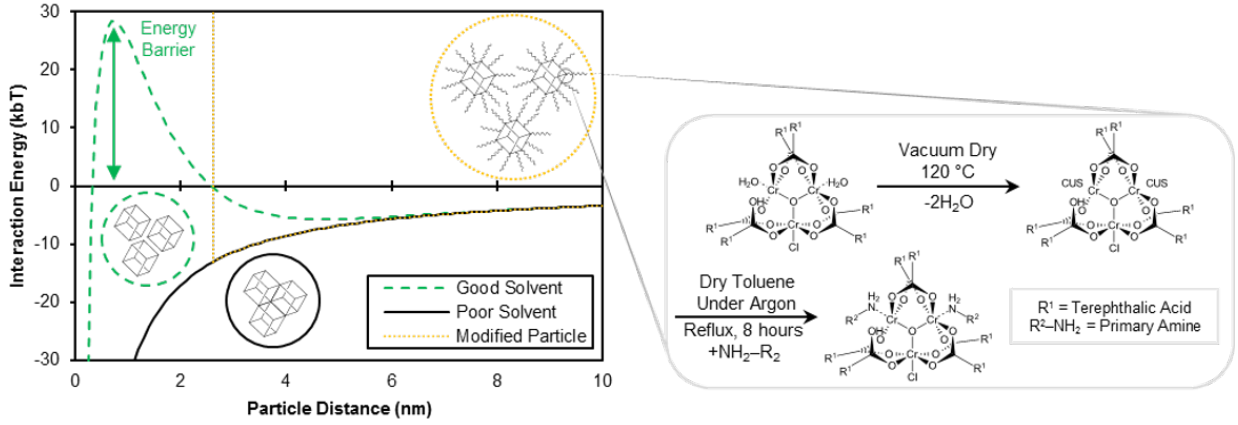

Figure 3: Colloidal theory following the classic and extended DLVO models along with the chemistry of the MIL-101 modification.

The theoretical predictions from DLVO theory correlate well with the measured aggregation behavior illustrated in Figure 4. The wavelength exponent is constant over regions that have similar particle sizes and decreases with increasing particle sizes.[34] Hence, as shown by Figure 4A, which relates to MIL-101, the critical point of aggregation is the point at which the two regions meet. The alcohol series in Figure 4B show that decreasing the solvent dielectric constant by increasing the alcohol chain length leads to lower critical points of aggregation. The picture becomes somewhat more complex when looking at a variety of functional groups.

Overall, as shown in Figure 4C, the solvents which provide better suspension of MIL-101 nanoparticles do indeed have higher dielectric constants: water, DMF, methanol (MeOH), acetone (Act), ethanol (EtOH) and n-butanol (BuOH). Moreover, aggregation is observed in most instances where the energy barrier ceases to exist, as is the case for DCM and n-hexane

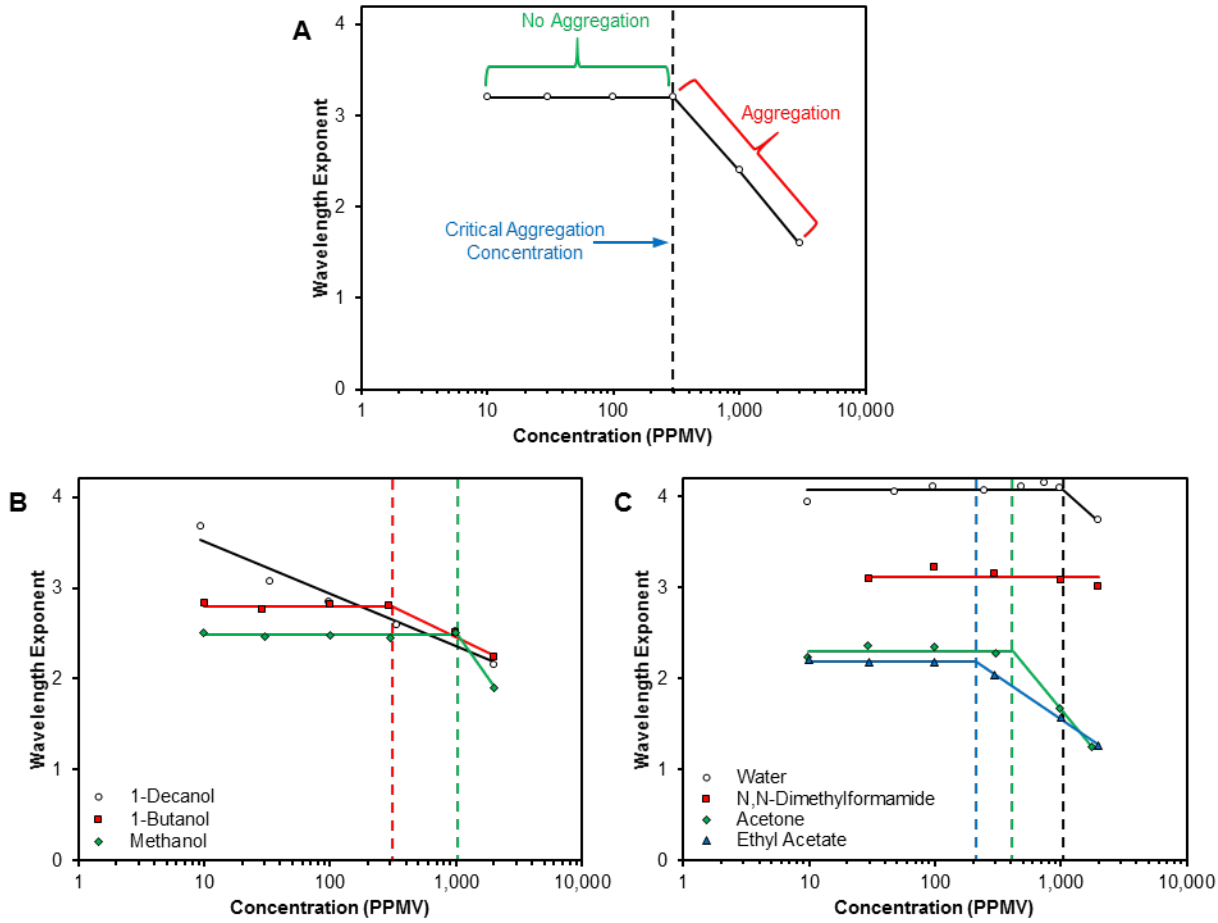

Figure 4: (A) Example of wavelength exponent versus concentration plot. (B & C) Wavelength exponent versus concentration plots for MIL-101 in select solvents.

(Hxn). Interestingly, while ethyl acetate (EA) shows no energy barrier, dilute suspensions are possible on the timescale of the measurements. Also, while the calculations suggest that water would be the best suspension solvent, DMF has a higher critical point of aggregation. These two observations could be related to acid-base interactions. Recent literature points toward this being a significant driver behind the colloidal behavior of MOFs.[35] DMF is a stronger base than water and EA is a stronger base than DCM and Hxn, as illustrated by their donicity.[36] Future work could focus on quantifying acid-base interactions, hydrophobic forces, hydrogen bonding and hydration pressure.[37] When it comes to formulation of products for monoliths based on MIL-101 and other similar MOFs, these data suggest that it would be best to use high dielectric constant solvents, perhaps those with high donicity

too. Regardless, stable suspensions of native MIL-101 are theoretically and observably unachievable in hydrophobic solvents such as DCM and Hxn. However, some applications or monolith fabrication techniques require the suspension of MOFs in hydrophobic solvents. This is for instance the case when developing thin film nanocomposite membranes or mixed matrix membranes. Indeed, these membranes eventually require good interactions between the polymeric component and the filler particles and moreover, their synthesis may involve hydrophobic solvents. The suspension of the fillers in such hydrophobic solvents will eventually influence their dispersion in the membranes and thereby the membranes' performance.

To achieve hydrophobic suspension, MIL-101 was modified post-synthetically by attaching octylamine (OA) and amine-terminated polystyrene (ATPS) to its coordinatively unsaturated sites. The X-ray diffraction (XRD) data (Figure 5A) illustrate that the crystalline structures of the modified MIL-101s remained unaffected by the modification procedures. The Fourier-transform infrared spectroscopy (FTIR) data (Figure 5B) are largely comparable between all samples with the exception of additional bands that correspond to the most intense peaks of OA and ATPS (Figure S1, Supporting Information). While these data demonstrate the presence of OA and ATPS, more conclusive evidence was found with X-ray photoelectron spectroscopy (XPS).

The compositional data of the modified samples measured via XPS are consistent with theoretical calculations (Figure S4, Supporting Information). Particularly, the increase in carbon and nitrogen for MIL-101 (OA) and MIL-101 (ATPS) are equivalent to the stoichiometric ratios of OA (8:1) and ATPS (770:1). A closer investigation of the spectra in the N1s region (Figure 5C) confirms the coordination of OA and ATPS to the coordinatively unsaturated sites of MIL-101. The peak at 400.4 eV in the MIL-101 control is attributable to DMF,[38] which is used in the activation procedure (Section S2.1, Supporting Information). This only accounts for a part of the total amine content in the modified samples. New peaks for MIL-101 (OA) and MIL-101 (ATPS) can be detected at 399.7 eV and 398.1 eV. Uncoordinated primary amines have a binding energies of at least 400.3 eV, whereas coordinated

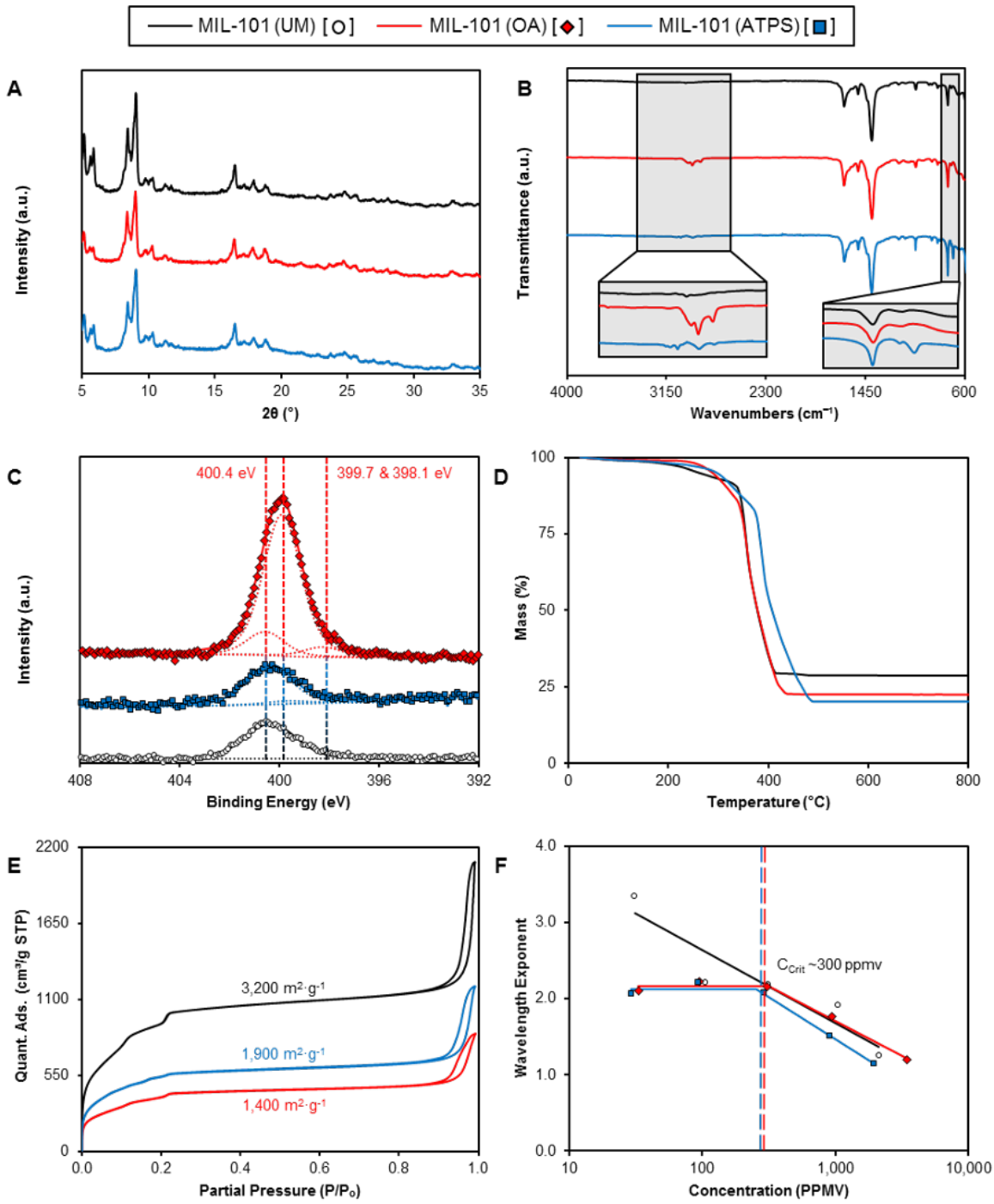

Figure 5: Characterization of modified and unmodified MIL-101: (A) XRD, (B) FTIR, (C) XPS, (D) nitrogen isotherm, (E) TGA and (F) wavelength exponent versus concentration. Vertical lines highlight peak binding energies, peak transmission energies and the critical point of aggregation in (B), (C) and (F), respectively. Respective BET surface areas are shown in (E).

amines have binding energies between 399.7 and 400.0 eV.[39] Thus, the peak at 399.7 eV strongly suggests that OA is coordinated to MIL-101. The smaller peak at 398.1 eV could be deprotonated OA.[39]

The degree of modification as a percent of the theoretical maximum can be calculated via XPS or thermogravimetric analysis (TGA) (Sections S3.5 and S3.6, Supporting Information). An estimated degree of modification of 69.7% for the MIL-101 (OA) was determined by XPS. This is ≈2% different than the degree of modification estimated via TGA: 71.2 ± 3.1% (95% confidence interval, n = 4) (Figure 5D, Section S3.5, Supporting Information), well within experimental error. Moreover, nitrogen sorption revealed a 58% reduction in the (Brunauer–Emmett–Teller) BET surface area. Even when mass-normalized to account for the OA, the BET surface area decreased by 46%. Since XPS is a surface sensitive technique and TGA/BET analyses measure bulk properties, these data indicate that the OA modification occurred both on MIL-101's surface and throughout its microporous structure. In contrast to the MIL-101 (OA), MIL-101 (ATPS) exhibited a surface-selective modification. The XPS revealed a 3.7% modification, which is 2.6 times larger and well outside the error of the TGA measurement: 1.4 ± 0.1% (95 % confidence interval, n = 4) (Figure 5D, Section S3.5, Supporting Information). This suggests a greater concentration of ATPS on MIL-101's surface than in its bulk. Moreover, the mass-normalized BET surface area loss was only 17%, within the error of analysis for nitrogen sorption. These data demonstrate that it is possible to achieve surface-selective modification of a MOF by using large molecules. As shown in Figure 5F, MIL-101 (OA) and MIL-101 (ATPS) gave better suspensions than native MIL-101 in a mixture of low-molecular weight alkane chains with a dielectric constant of ≈2 (IsoPar G). Instead of observing aggregation across the entire measured range, up to ≈300 ppmv of MIL-101 could be suspended in solution. This can be modelled by adding a steric repulsion term to the classic DLVO equation, which requires the areal mass density of the surface coating alongside a number of other values from the literature (Section S1.3). Figure 3 demonstrates such a calculation, showing a strong steric repulsive force at twice the length

of the molecule used for modification. One advantage to grafting mono-terminated amines to the coordinatively unsaturated sites of MIL-101 is that the product can be synthesized, modified and stored in a dry powder format for subsequent re-suspension (Section S2). Also, the ability to independently modify the internal pore structure and particle envelop of a MOF could enable interesting applications not explored in this work. While the MIL-101 (OA) is relatively hydrophobic throughout its pore structure, the MIL-101 (ATPS) retains MIL-101's natural textural and chemical properties while generating a hydrophobic shell that causes MIL-101 (ATPS) to float on water – an unusual phenomena for a MOF so hydrophilic that it makes a crackling sound when added to water.

4 Conclusions

In conclusion, the interparticle van der Waals attractive forces of MOF nanoparticles in various solvent environments were determined for the first time and found to be relatively low. Thus, colloidal suspensions were achieved in high dielectric constant solvents via electric double layer repulsive forces, as described by DLVO theory. However, the electric double layer repulsive forces diminish in low dielectric constant solvents, leading to unstable suspensions. To ameliorate this challenge, MIL-101 particles were post-synthetically modified by grafting non-selective and surface-selective hydrophobic molecules to their coordinatively unsaturated sites. The grafted molecules induced steric repulsion, enabling uniform suspension of MIL-101 nanoparticles in a hydrophobic solvent. Using the values determined in this work, it is possible to predict the suspension of MIL-101 in any solvent using an extended DLVO theory. This should greatly faciliate the systematic preparation of colloidal dispersions of MOFs, thus supporting MOF application and device fabrication.

Supporting Information Available

The Supporting Information contains: a list of abbreviations, a short background on colloid science theory, details on materials synthesis, modification, suspension and film fabrication, analyses of MOF powder characterization, analyses of MOF colloidal characterization, and analyses of MOF film characterization.

Acknowledgement

The authors thank the Marshall Aid Commemoration Commission and the Environmental Protection Agency supported this work. Dr. Vladimir Martis at Surface Measurement Systems Ltd. conducted the dynamic vapour sorption (DVS vacuum) measurements.

References

(1) Furukawa, H.; Cordova, K. E.; O'Keeffe, M.; Yaghi, O. M. The Chemistry and Applications of Metal-Organic Frameworks. *Science* **2013**, *341*.

(2) Yuan, S.; Feng, L.; Wang, K.; Pang, J.; Bosch, M.; Lollar, C.; Sun, Y.; Qin, J.; Yang, X.; Zhang, P.; Wang, Q.; Zou, L.; Zhang, Y.; Zhang, L.; Fang, Y.; Li, J.; Zhou, H.-C. Stable Metal-Organic Frameworks: Design, Synthesis, and Applications. *Adv. Mater.* **2018**, *30*.

(3) Meng, J.; Liu, X.; Niu, C.; Pang, Q.; Li, J.; Liu, F.; Liu, Z.; Mai, L. Advances in metal-organic framework coatings: versatile synthesis and broad applications. *Chem. Soc. Rev.* **2020**, *49*, 3142–3186.

(4) Qiu, T.; Liang, Z.; Guo, W.; Tabassum, H.; Gao, S.; Zou, R. MetalâOrganic Framework-Based Materials for Energy Conversion and Storage. *ACS Energy Letters* **2020**, *5*, 520–532.

(5)

(6) Ryu, U.; Jee, S.; Rao, P. C.; Shin, J.; Ko, C.; Yoon, M.; Park, K. S.; Choi, K. M. Recent advances in process engineering and upcoming applications of metal-organic frameworks. *Coordination Chemistry Reviews* **2021**, *426*, 213544.

(7) Horcajada, P.; Chalati, T.; Serre, C.; Gillet, B.; Sebrie, C.; Baati, T.; Eubank, J. F.; Heurtaux, D.; Clayette, P.; Kreuz, C.; Chang, J. S.; Hwang, Y. K.; Marsaud, V.; Bories, P. N.; Cynober, L.; Gil, S.; Férey, G.; Couvreur, P.; Gref, R. Porous Metal-Organic-Framework Nanoscale Carriers as a Potential Platform for Drug Deliveryand Imaging. *Nat. Mater.* **2010**, *9*, 172–178.

(8) Lee, J.; Farha, O. K.; Roberts, J.; Scheidt, K. A.; Nguyen, S. T.; Hupp, J. T. Metal-Organic Framework Materials as Catalysts. *Chem. Soc. Rev.* **2009**, *38*, 1450–1459.

(9) Adil, K.; Belmabkhout, Y.; Pillai, R. S.; Cadiau, A.; Bhatt, P. M.; Assen, A. H.; Maurin, G.; Eddaoudi, M. Gas/Vapour Separation using Ultra-Microporous Metal-Organic Frameworks: Insights into the Structure/Separation Relationship. *Chem. Soc. Rev.* **2017**, *46*, 3402–3430.

(10) Zornoza, B.; Tellez, C.; Coronas, J.; Gascon, J.; Kapteijn, F. Metal Organic Framework Based Mixed Matrix Membranes: An Increasingly Important Field of Research with a Large Application Potential. *Microporous Mesoporous Mater.* **2013**, *166*, 67–78.

(11) Stassen, I.; Burtch, N.; Talin, A.; Falcaro, P.; Allendorf, M.; Ameloot, R. An Updated Roadmap for the Integration of Metal-Organic Frameworks with Electronic Devices and Chemical Sensors. *Chem. Soc. Rev.* **2017**, *46*, 3185–3241.

(12) Lustig, W. P.; Mukherjee, S.; Rudd, N. D.; Desai, A. V.; Li, J.; Ghosh, S. K. Metal-Organic Frameworks: Functional Luminescent and Photonic Materials for Sensing Applications. *Chem. Soc. Rev.* **2017**, *46*, 3242–3285.

(13) Wang, S.; Morris, W.; Liu, Y.; McGuirk, C. M.; Zhou, Y.; Hupp, J. T.; Farha, O. K.; Mirkin, C. A. Surface-Specific Functionalization of Nanoscale Metal-Organic Frameworks. *Angew. Chemie* **2015**, *127*, 14951–14955.

(14) Lu, G.; Li, S.; Guo, Z.; Farha, O. K.; Hauser, B. G.; Qi, X.; Wang, Y.; Wang, X.; Han, S.; Liu, X.; Duchene, J. S.; Zhang, H.; Zhang, Q.; Chen, X.; Ma, J.; Loo, S. C. J.; Wei, W. D.; Yang, Y.; Hupp, J. T.; Huo, F. Imparting Functionality to a Metal-Organic Framework Material by Controlled Nanoparticle Encapsulation. *Nat. Chem.* **2012**, *4*, 310–316.

(15) Yanai, N.; Granick, S. Directional Self-Assembly of a Colloidal Metal-Organic Framework. *Angew. Chemie - Int. Ed.* **2012**, *51*, 5638–5641.

(16) Dalstein, O.; Gkaniatsou, E.; Sicard, C.; Sel, O.; Perrot, H.; Serre, C.; Boissière, C.; Faustini, M. Evaporation-Directed Crack-Patterning of Metal-Organic Framework Colloidal Films and Their Application as Photonic Sensors. *Angew. Chemie* **2017**, *129*, 14199–14203.

(17) Demessence, A.; Horcajada, P.; Serre, C.; Boissière, C.; Grosso, D.; Sanchez, C.; Férey, G. Elaboration and Properties of Hierarchically Structured Optical Thin Films of MIL-101(Cr). *Chem. Commun.* **2009**, 7149–7151.

(18) Férey, C.; Mellot-Draznieks, C.; Serre, C.; Millange, F.; Dutour, J.; Surblé, S.; Margiolaki, I. Chemistry: A Chromium Terephthalate-Based Solid with Unusually Large Pore Volumes and Surface Area. *Science* **2005**, *309*, 2040–2042.

(19) Khan, N. A.; Kang, I. J.; Seok, H. Y.; Jhung, S. H. Facile synthesis of nano-sized metal-organic frameworks, chromium-benzenedicarboxylate, MIL-101. *Chem. Eng. J.* **2011**, *166*, 1152–1157.

(20) Sorribas, S.; Gorgojo, P.; Téllez, C.; Coronas, J.; Livingston, A. G. High Flux Thin Film

Nanocomposite Membranes Based on Metal–Organic Frameworks for Organic Solvent Nanofiltration. *J. Am. Chem. Soc.* **2013**, *135*, 15201–15208.

(21) Brunauer, S.; Emmett, P. H.; Teller, E. Adsorption of Gases in Multimolecular Layers. *J. Am. Chem. Soc.* **1938**, *60*, 309–319.

(22) Hunter, R. J. *Zeta Potential in Colloid Science - Principles and Applications*; Academic Press, 1981; pp 59–124.

(23) Heller, W.; Vassy, E. Tyndall Spectra, their Significance and Application. *J. Chem. Phys.* **1946**, *14*, 565–566.

(24) Heller, W.; McCarty, H. Theoretical Investigations on the Light Scattering of Colloidal Spheres .4. Specific Turbidities in the Lower Microscopic Range and Fine Structure Phenomena. *J. Chem. Phys.* **1958**, *29*, 78–80.

(25) Heller, W.; Bhatnagar, H. L.; Nakagaki, M. Theoretical Investigations on the Light Scattering of Spheres. XIII. The "Wavelength Exponent" of Differential Turbidity Spectra. *J. Chem. Phys.* **1962**, *36*, 1163–1170.

(26) Long, J.; Osmond, D.; Vincent, B. The equilibrium aspects of weak flocculation. *J. Colloid Interface Sci.* **1973**, *42*, 545–553.

(27) Reid, B.; Taylor, A.; Chen, Y.; Schmidt-Hansberg, B.; Guldin, S. Robust Operation of Mesoporous Antireflective Coatings under Variable Ambient Conditions. *ACS Appl. Mater. Interfaces* **2018**, *10*, 10315–10321.

(28) Boissiere, C.; Grosso, D.; Lepoutre, S.; Nicole, L.; Bruneau, A. B.; Sanchez, C. Porosity and Mechanical Properties of Mesoporous Thin Films Assessed by Environmental Ellipsometric Porosimetry. *Langmuir* **2005**, *21*, 12362–12371.

(29) Alvarez-Fernandez, A.; Reid, B.; Fornerod, M. J.; Taylor, A.; Divitini, G.; Guldin, S.

Structural Characterization of Mesoporous Thin Film Architectures: A Tutorial Overview. *ACS Appl. Mater. Interfaces* **2020**, *12*, 5195–5208.

(30) Sing, K. S. Reporting Physisorption Data for Gas/Solid Systems. *Pure Appl. Chem.* **1982**, *54*, 2201–2218.

(31) Eslava, S.; Baklanov, M. R.; Kirschhock, C. E. A.; Iacopi, F.; Aldea, S.; Maex, K.; Martens, J. A. Characterization of a molecular sieve coating using ellipsometric porosimetry. *Langmuir* **2007**, *23*, 12811–12816.

(32) Pan, S.; Richardson, J. J.; Christofferson, A. J.; Besford, Q. A.; Zheng, T.; Wood, B. J.; Duan, X.; Jara Fornerod, M. J.; McConville, C. F.; Yarovsky, I.; Guldin, S.; Jiang, L.; Caruso, F. Fluorinated Metal–Organic Coatings with Selective Wettability. *J. Am. Chem. Soc.* **2021**, *143*, 9972–9981.

(33) Bergström, L. Hamaker Constants of Inorganic Materials. *Adv. Colloid Interface Sci.* **1997**, *70*, 125–169.

(34) Heller, W. The Determination of Refractive Indices of Colloidal Particles by Means of a New Mixture Rule or from Measurements of Light Scattering. *Phys. Rev.* **1945**, *68*, 5–10.

(35) Lai, Y. C.; Kung, C. W.; Su, C. H.; Ho, K. C.; Liao, Y. C.; Tsai, D. H. Metal-Organic Framework Colloids: Disassembly and Deaggregation. *Langmuir* **2016**, *32*, 6123–6129.

(36) Cataldo, F. A Revision of the Gutmann Donor Numbers of a Series of Phosphoramides Including TEPA. *Eur. Chem. Bull.* **2015**, *4*, 92–97.

(37) Grasso, D.; Subramaniam, K.; Butkus, M.; Strevett, K.; Bergendahl, J. A Review of non-DLVO Interactions in Environmental Colloidal Systems. *Rev. Environ. Sci. Biotechnol.* **2002**, *1*, 17–38.

(38) Nefedov, V. I.; Salyn, Y. V.; Shtemenko, A. V.; Kotelnikova, A. S. X-ray Photoelectron Study of Trans-Influence of the Re-Re Multiple Bond. *Inorganica Chim. Acta* **1980**, *45*, L49–L50.

(39) Inamura, K.; Inoue, Y.; Ikeda, S.; Kishi, K. X-Ray Photoelectron Spectroscopic Study for the Adsorption and the Decomposition of Alkylamines on Nickel. *Surf. Sci.* **1985**, *155*, 173–186.

Graphical TOC Entry